# Supplemental: Seasonal variation in size-resolved particle deposition and the effect of environmental conditions on dry deposition in a pine forest

Erin K. Boedicker[a], Holly M. DeBolt[a], Ryan Fulgam[a,*], Ethan W. Emerson[a,b], and Delphine K. Farmer[a]

[a]Department of Chemistry, Colorado State University, Fort Collins, CO, USA; [b]Handix Scientific, Fort Collins, CO, USA

* Now at Environmental Protection Agency, Durham, North Carolina, USA

*Correspondence to*: Delphine K. Farmer Delphine.Farmer@colostate.edu Department of Chemistry, Colorado State University, 1301 Center Ave, Fort Collins, CO, 80523, USA.

**Number of pages:** 15
**Number of figures:** 15
**Number of tables:** 3

**CONTENTS**

**Section S1: Site Set-up and Meteorological Parameters During the Campaign Periods**

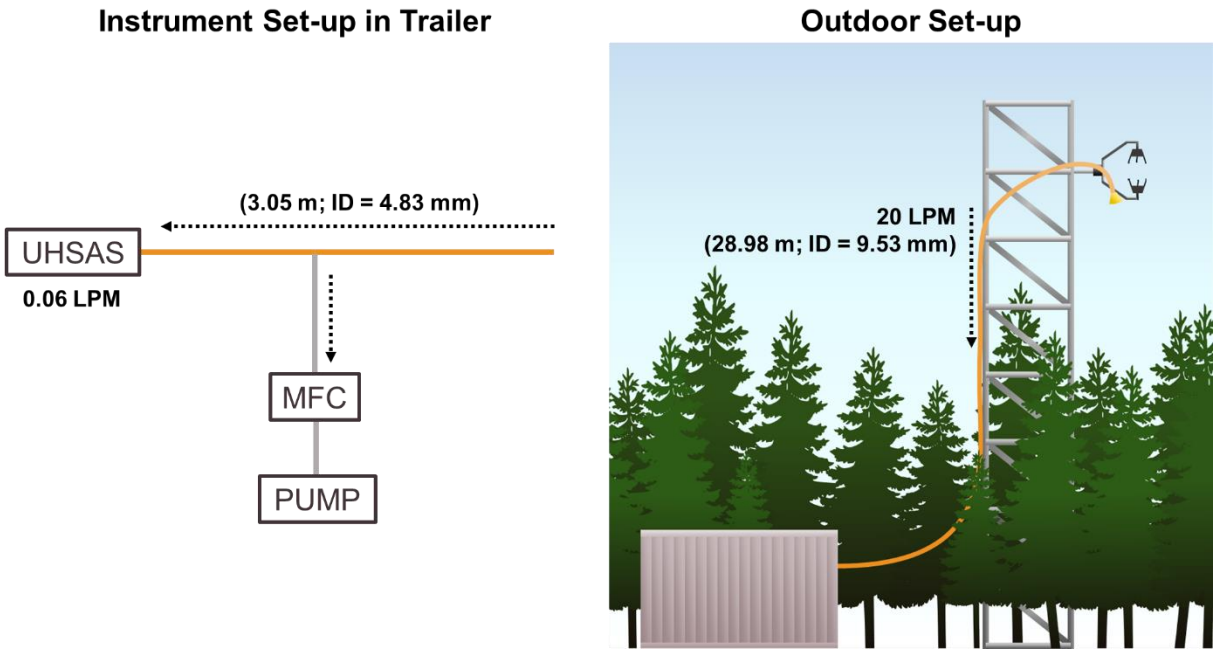


**Figure S1**: Schematic of the instrument set up at the Manitou Experimental Forest Observatory.

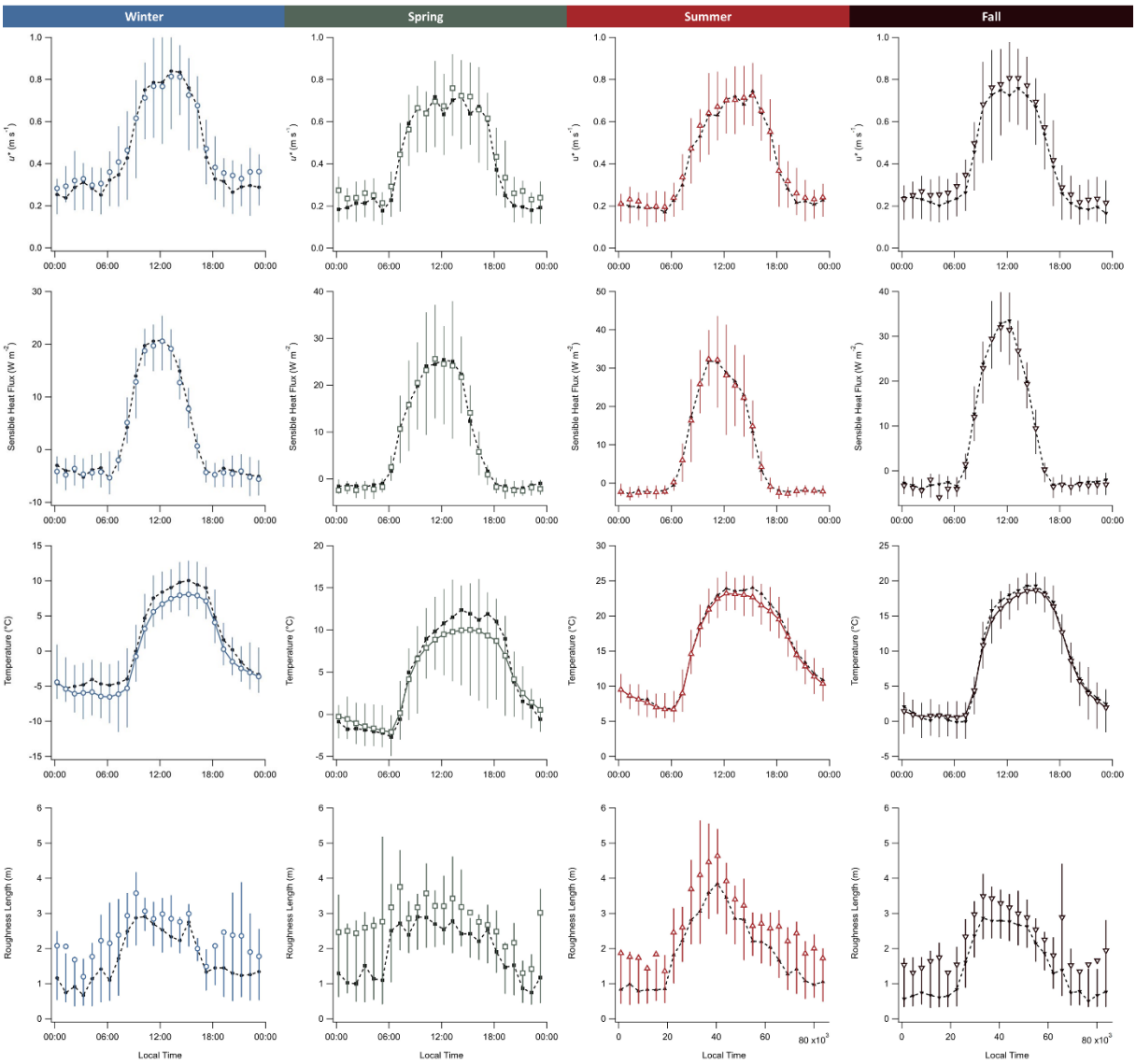


**Figure S2**: Average diel cycle for friction velocity ($u^*$), sensible heat flux ($H$), air temperature, and roughness length of each season. Open points are means, while the error bars represent the 25$^{th}$ and 75$^{th}$ percentiles, and the solid points represent the medians.

**Section S2: Results from eddy-covariance analysis and derived relationships between model variables**

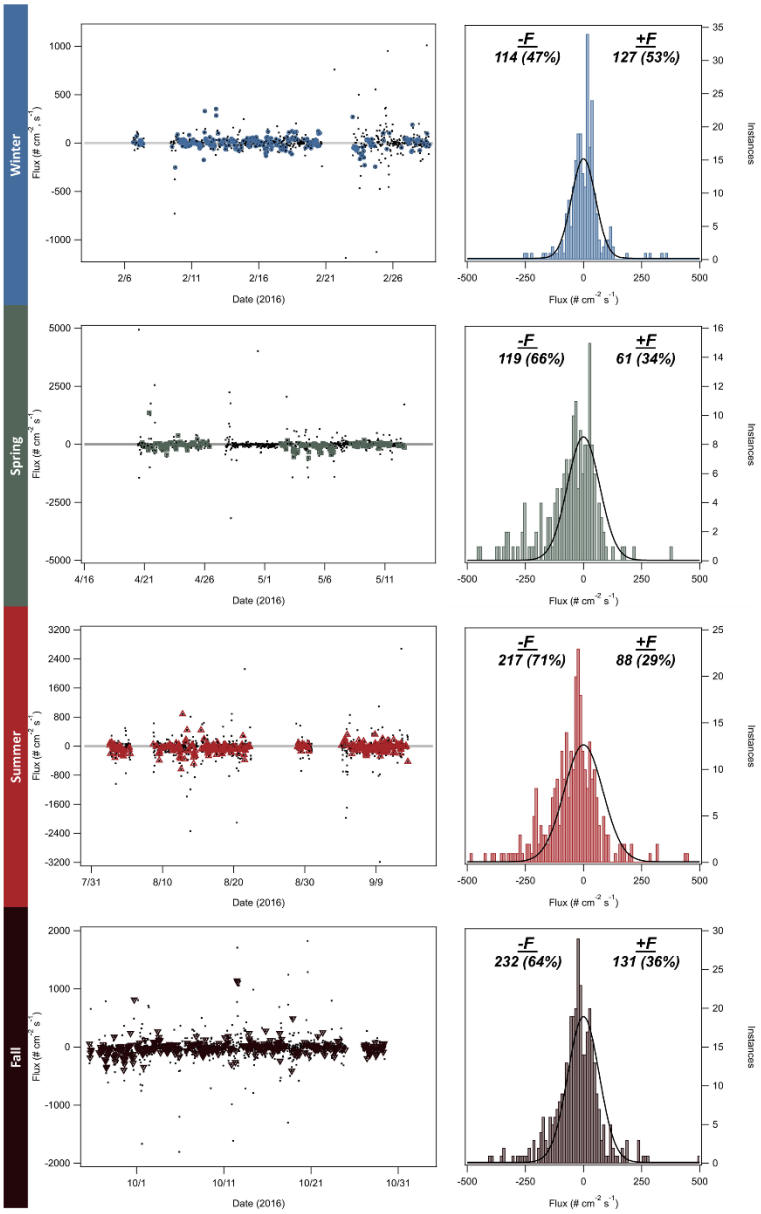


**Figure S3:** Graphical results of flux QC filtering (left) along with a histogram of flux instances (right). In the timeseries of QC filtering the black points are all available flux periods and the colored markers are the periods that passed all QC parameters listed in **Section 2.3.1**. The histogram for each season shows visually unequal distributions of flux instances about zero (number of positive and negative fluxes are also provided). In addition to visual investigation, a Kolmogorov-Smirnov test on the data from all seasons resulted in the rejection of the hypothesis that the data was taken from a normal distribution. Indicating that the positive and negative fluxes can be treated separately as source emissions and deposition.

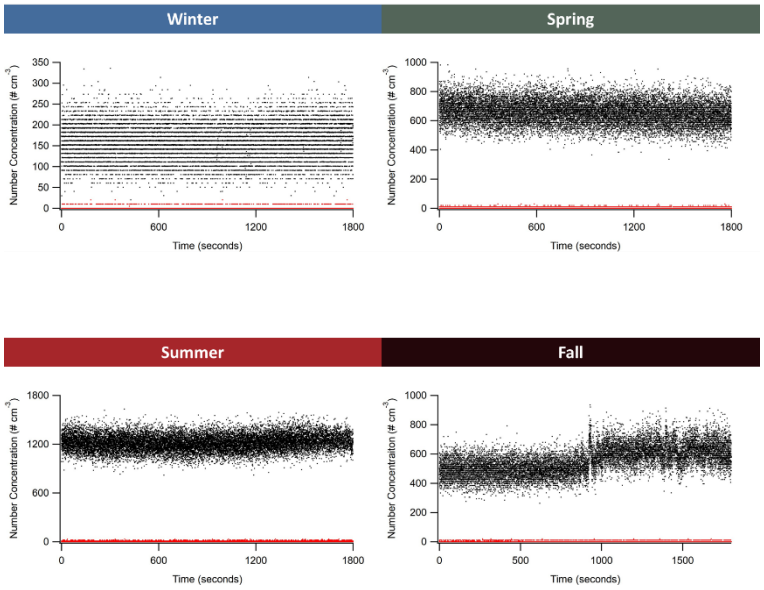


**Figure S4**: Calculation of the SNR for each seasonal measurement period. With the black data representing the 30 minutes of data before a system filter and the red data representing the data from the adjacent 30-minute filtering period.

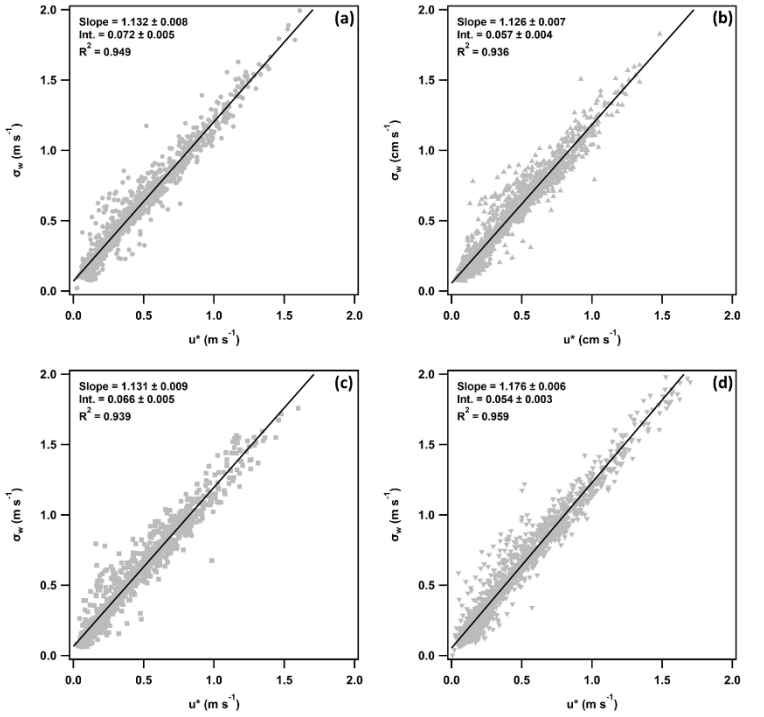


**Figure S5**: Relationship between the standard deviation of the vertical velocity ($\sigma_w$) and friction velocity ($u$*) for the (a) winter, (b) spring, (c) summer, and (d) fall.

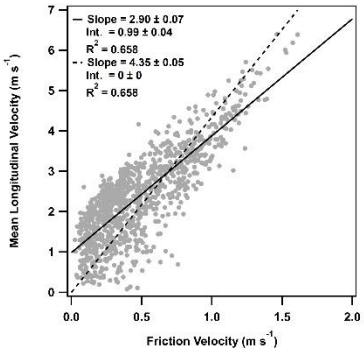


**Figure S6**: Relationship of the mean longitudinal velocity ($\overline{U}$) to the friction velocity ($u^*$) for the winter SPiFFY data.

## Section S3: Seasonal trends in flux, exchange velocity, and concentration and variation in particle size distributions

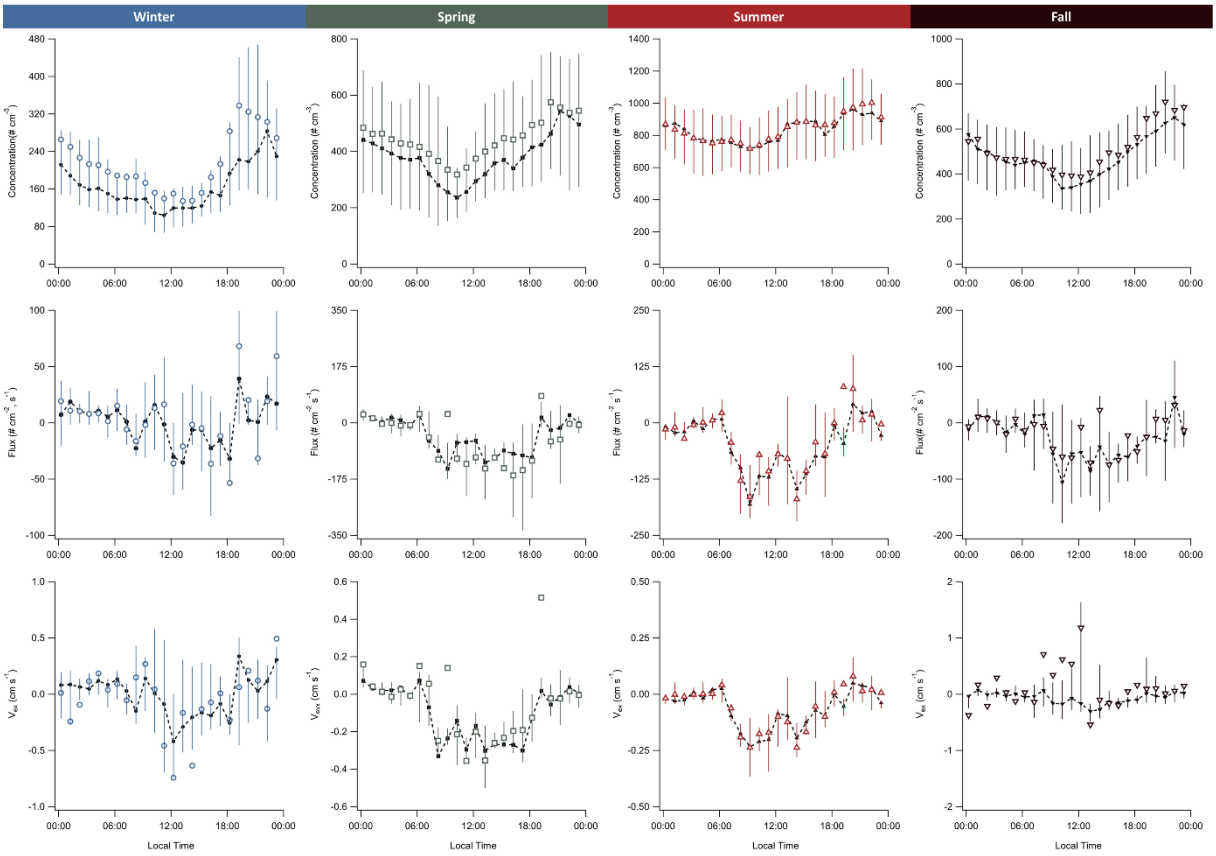


**Figure S7**: Diel trends of number concentration, flux, and exchange velocity ($V_{ex}$) for each season. Open points are means, while the error bars represent the 25$^{th}$ and 75$^{th}$ percentiles, and the solid points represent the medians.

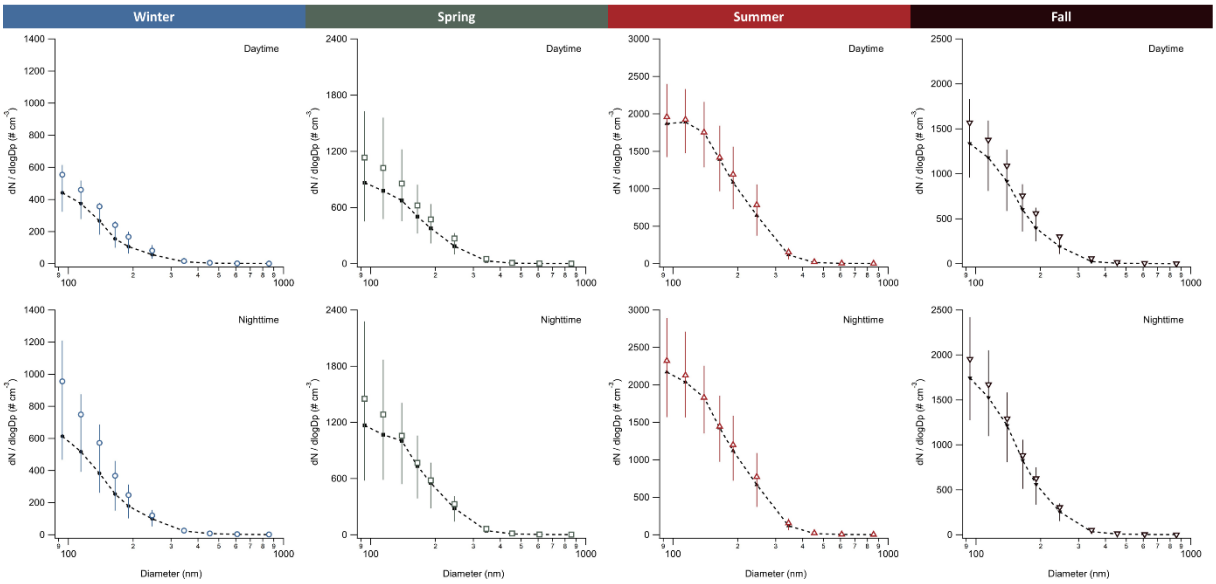


**Figure S8**: Daytime (top row) and nighttime (bottom row) particle size distributions for each seasonal period. These periods were defined using average reported sunrise and sunset times. Open points are means, while the error bars represent the 25$^{th}$ and 75$^{th}$ percentiles, and the solid points represent the medians.

**Table S1**: Count median diameters (CMD), as well as surface median diameters (SMD), volume median diameters (VMD), and the geometric standard deviation (GSD) for the daytime and nighttime particle distributions of each season.

| Diameter Type | Period | Winter | Spring | Summer | Fall |
|---|---|---|---|---|---|
| CMD | Daytime | 129 ± 8 | 140 ± 20 | 140 ± 10 | 130 ± 10 |
| | Nighttime | 129 ± 7 | 140 ± 20 | 140 ± 10 | 128 ± 7 |
| SMD | Daytime | 160 ± 20 | 170 ± 30 | 180 ± 20 | 160 ± 20 |
| | Nighttime | 160 ± 20 | 170 ± 30 | 180 ± 20 | 160 ± 10 |
| VMD | Daytime | 180 ± 20 | 190 ± 30 | 200 ± 30 | 170 ± 20 |
| | Nighttime | 180 ± 20 | 200 ± 40 | 200 ± 30 | 170 ± 20 |
| GSD | Daytime | 1.38 ± 0.04 | 1.38 ± 0.04 | 1.42 ± 0.05 | 1.37 ± 0.04 |
| | Nighttime | 1.39 ± 0.05 | 1.39 ± 0.05 | 1.42 ± 0.06 | 1.37 ± 0.04 |

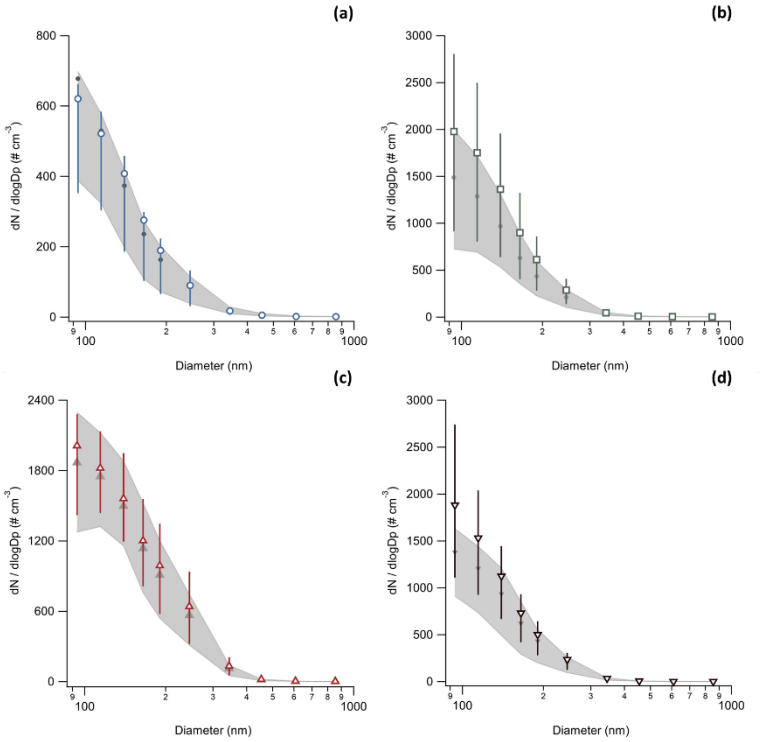


**Figure S9**: Comparison of particle size-distributions between periods of positive and negative flux measurements for the (**a**) winter, (**b**) spring, (**c**) summer, and (**d**) fall. In each figure the grey points and shading represent the mean concentration and the 25$^{th}$ and 75$^{th}$ percentiles for periods where a positive flux was observed, while the colored points and lines represent the mean concentration and the 25$^{th}$ and 75$^{th}$ percentiles for periods where a negative flux was observed.

**Table S2**: Count median diameters (CMD), surface median diameters (SMD), volume median diameters (VMD), and the geometric standard deviation (GSD) for particle distributions during positive and negative particle flux measurement periods.

| Diameter Type | Flux Type | Winter | Spring | Summer | Fall |
|---|---|---|---|---|---|
| CMD | + Flux | 128 ± 8 | 129 ± 6 | 140 ± 10 | 129 ± 8 |
| | - Flux | 129 ± 9 | 129 ± 4 | 140 ± 10 | 128 ± 7 |
| SMD | + Flux | 160 ± 20 | 160 ± 10 | 180 ± 20 | 160 ± 20 |
| | - Flux | 160 ± 20 | 157 ± 9 | 180 ± 20 | 160 ± 10 |
| VMD | + Flux | 180 ± 20 | 180 ± 10 | 200 ± 30 | 180 ± 20 |
| | - Flux | 180 ± 20 | 170 ± 10 | 200 ± 30 | 170 ± 20 |
| GSD | + Flux | 1.38 ± 0.05 | 1.37 ± 0.03 | 1.40 ± 0.04 | 1.37 ± 0.04 |
| | - Flux | 1.38 ± 0.04 | 1.37 ± 0.03 | 1.40 ± 0.04 | 1.36 ± 0.03 |

**Section S4: Seasonal trends in deposition velocity and model comparisons**

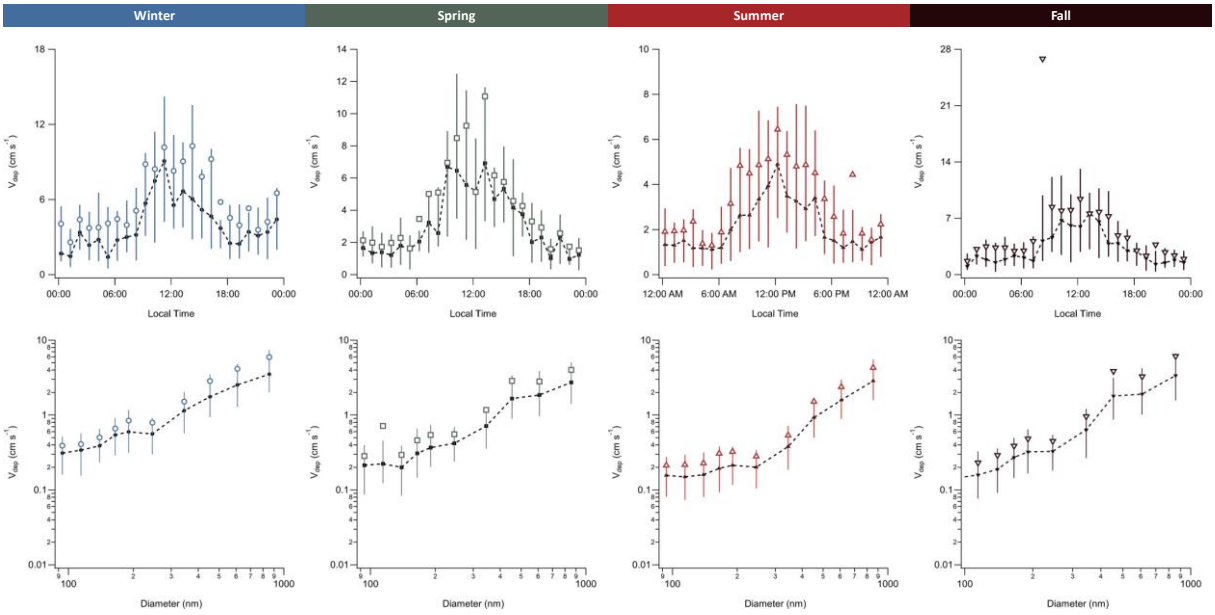


**Figure S10**: Seasonal total (top row) size-dependent (bottom row) deposition velocities for the winter, spring, summer, and fall. Open points are means, while the error bars represent the 25$^{th}$ and 75$^{th}$ percentiles, and the solid points represent the medians.

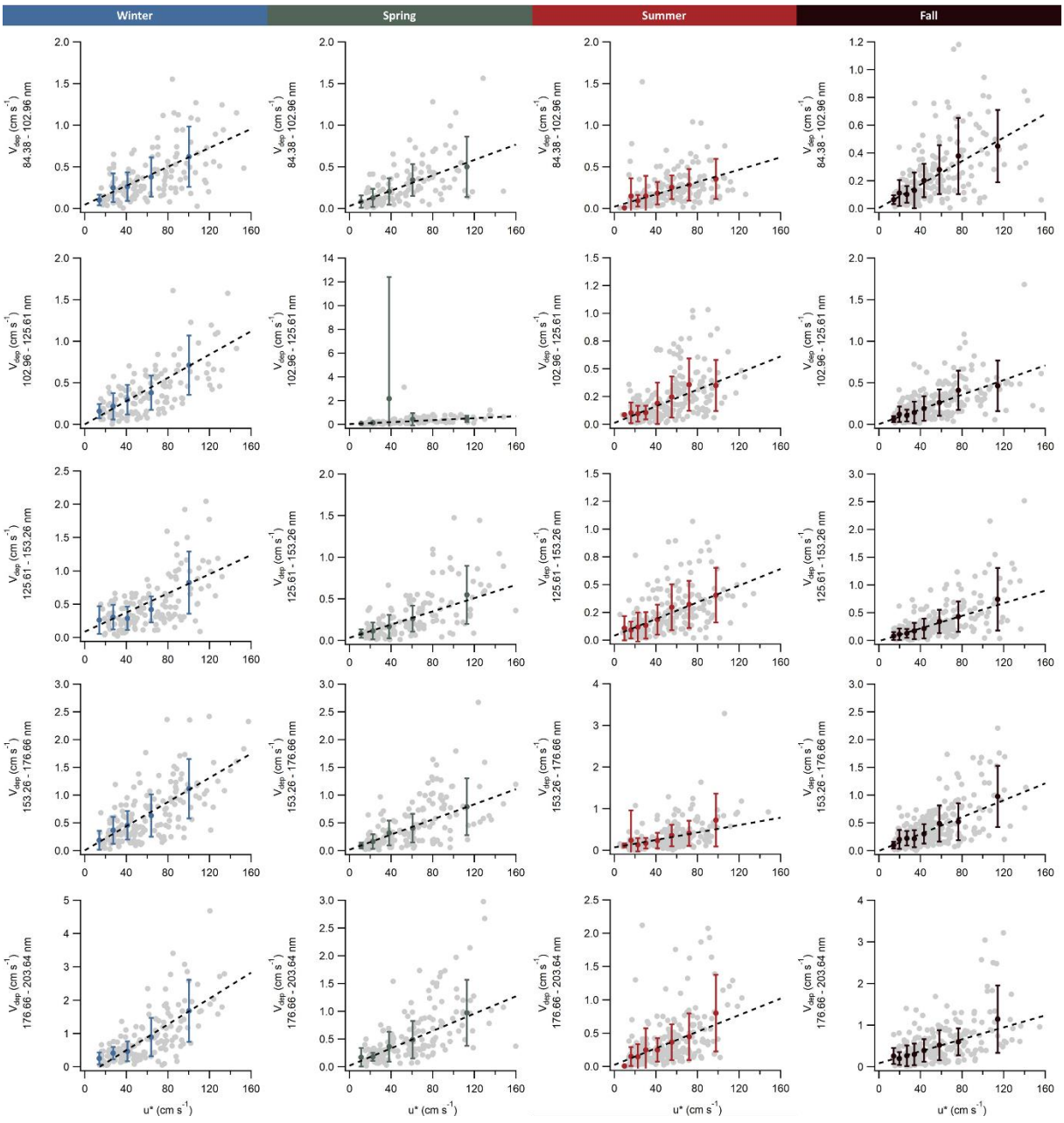
Winter
Spring
Summer
Fall
$V_{dep}$ (cm s$^{-1}$) 84.38 - 102.96 nm
$V_{dep}$ (cm s$^{-1}$) 102.96 - 125.61 nm
$V_{dep}$ (cm s$^{-1}$) 125.61 - 153.26 nm
$V_{dep}$ (cm s$^{-1}$) 153.26 - 176.66 nm
$V_{dep}$ (cm s$^{-1}$) 176.66 - 203.64 nm
u* (cm s$^{-1}$)

90

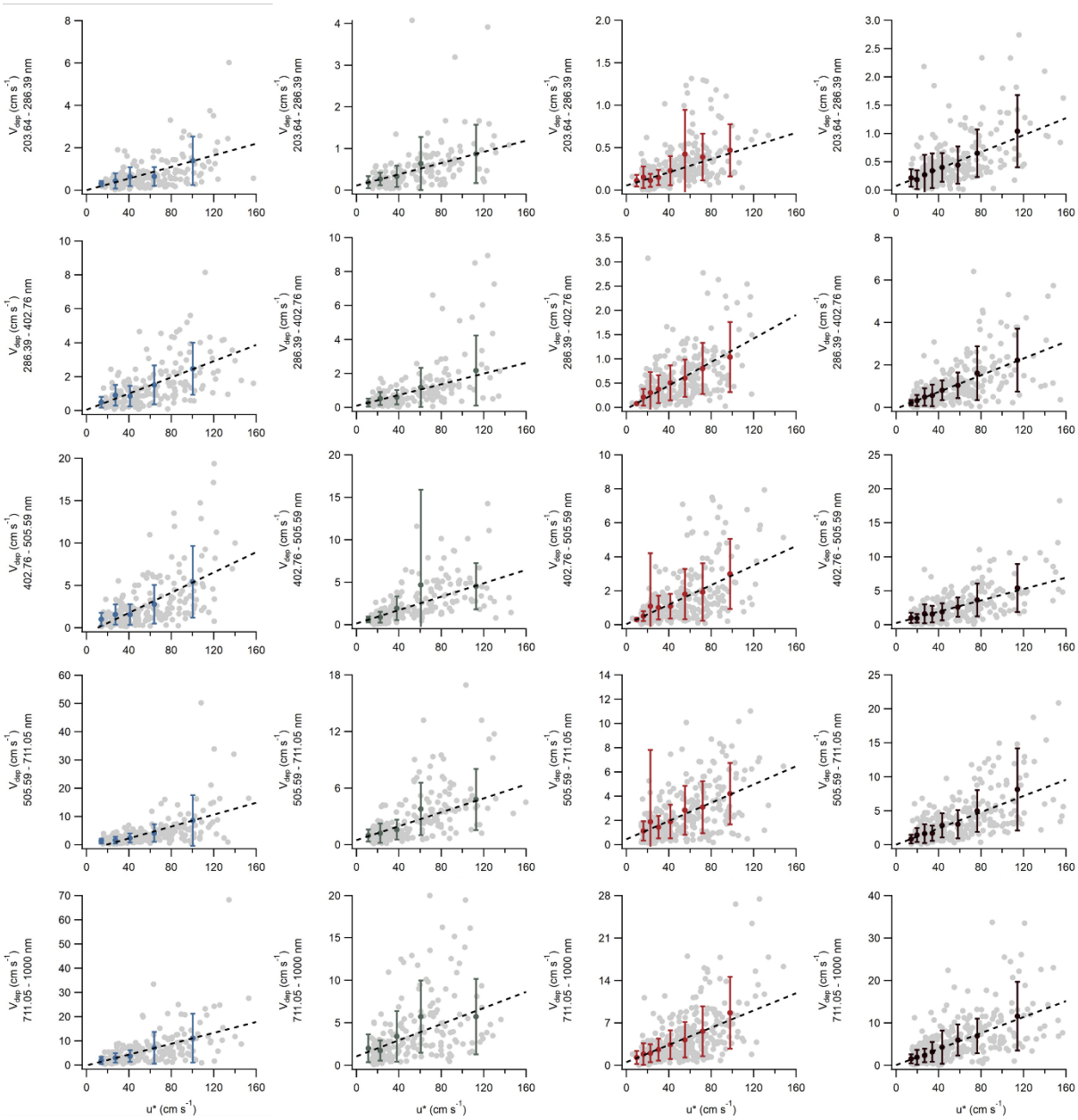


**Figure S11**: Seasonal size-dependent deposition velocities compared to friction velocity ($u^*$) for the winter, spring, summer, and fall. Grey points represent raw data and colored points represent data binned by $u^*$, with each point representing 200 measurement periods (periods removed during quality control are included in count but not comparison).

**Table S3**: Linear fits to the size-dependent deposition velocities versus friction velocity ($u^*$) for the winter, spring, summer, and fall.

| Size range (nm) | | Winter | Spring | Summer | Fall |
|---|---|---|---|---|---|
| 84.38 – 102.96 | Slope : | 0.01 ± 0.07 | 0.005 ± 0.003 | 0.004 ± 0.002 | 0.004 ± 0.002 |
| | Int. : | 1 ± 6 | 0.03 ± 0.08 | 0.1 ± 0.1 | 0.01 ± 0.05 |
| | $R^2$ : | 0.693 | 0.861 | 0.888 | 0.799 |
| 102.96 – 125.61 | Slope : | 0.01 ± 0.07 | 0.004 ± 0.002 | 0.004 ± 0.002 | 0.004 ± 0.002 |
| | Int. : | -1 ± 6 | 0.03 ± 0.06 | 0.01 ± 0.08 | 0.01 ± 0.05 |

| | | | | | |
|---|---|---|---|---|---|
| | $R^2$ : | 0.836 | 0.042 | 0.826 | 0.802 |
| 125.61 – 153.26 | Slope : | 0.01 ± 0.04 | 0.004 ± 0.002 | 0.004 ± 0.002 | 0.006 ± 0.003 |
| | Int. : | 1 ± 4 | 0.03 ± 0.06 | 0.04 ± 0.07 | -0.01 ± 0.08 |
| | $R^2$ : | 0.827 | 0.688 | 0.856 | 0.637 |
| 153.26 – 176.66 | Slope : | 0.01 ± 0.04 | 0.007 ± 0.003 | 0.004 ± 0.003 | 0.008 ± 0.003 |
| | Int. : | 1 ± 3 | 0.02 ± 0.07 | 0.07 ± 0.06 | -0.01 ± 0.08 |
| | $R^2$ : | 0.862 | 0.804 | 0.496 | 0.675 |
| 176.66 – 203.64 | Slope : | 0.02 ± 0.04 | 0.008 ± 0.005 | 0.006 ± 0.004 | 0.007 ± 0.004 |
| | Int. : | -1 ± 3 | 0.1 ± 0.1 | 0.1 ± 0.2 | 0.1 ± 0.2 |
| | $R^2$ : | 0.798 | 0.819 | 0.633 | 0.578 |
| 203.64 – 286.39 | Slope : | 0.01 ± 0.03 | 0.007 ± 0.006 | 0.004 ± 0.003 | 0.007 ± 0.004 |
| | Int. : | -1 ± 2 | 0.1 ± 0.2 | 0.05 ± 0.07 | 0.1 ± 0.2 |
| | $R^2$ : | 0.720 | 0.786 | 0.628 | 0.748 |
| 286.39 – 402.76 | Slope : | 0.02 ± 0.02 | 0.02 ± 0.01 | 0.012 ± 0.004 | 0.020 ± 0.008 |
| | Int. : | 1 ± 1 | 0.1 ± 0.3 | -0.04 ± 0.04 | -0.1 ± 0.2 |
| | $R^2$ : | 0.774 | 0.580 | 0.936 | 0.707 |
| 402.76 – 505.59 | Slope : | 0.060 ± 0.008 | 0.04 ± 0.02 | 0.03 ± 0.01 | 0.04 ± 0.02 |
| | Int. : | -0.6 ± 0.7 | 0.1 ± 0.5 | 0.1 ± 0.2 | 0.2 ± 0.7 |
| | $R^2$ : | 0.841 | 0.518 | 0.759 | 0.722 |
| 505.59 – 711.05 | Slope : | 0.105 ± 0.006 | 0.04 ± 0.03 | 0.04 ± 0.02 | 0.06 ± 0.03 |
| | Int. : | -2.0 ± 0.5 | 0.5 ± 0.7 | 1 ± 1 | -0.1 ± 0.8 |
| | $R^2$ : | 0.833 | 0.720 | 0.839 | 0.579 |
| 711.05 - 1000 | Slope : | 0.112 ± 0.004 | 0.05 ± 0.04 | 0.07 ± 0.04 | 0.09 ± 0.04 |
| | Int. : | -0.2 ± 0.3 | 1 ± 1 | 1 ± 1 | 1 ± 1 |
| | $R^2$ : | 0.673 | 0.775 | 0.696 | 0.728 |

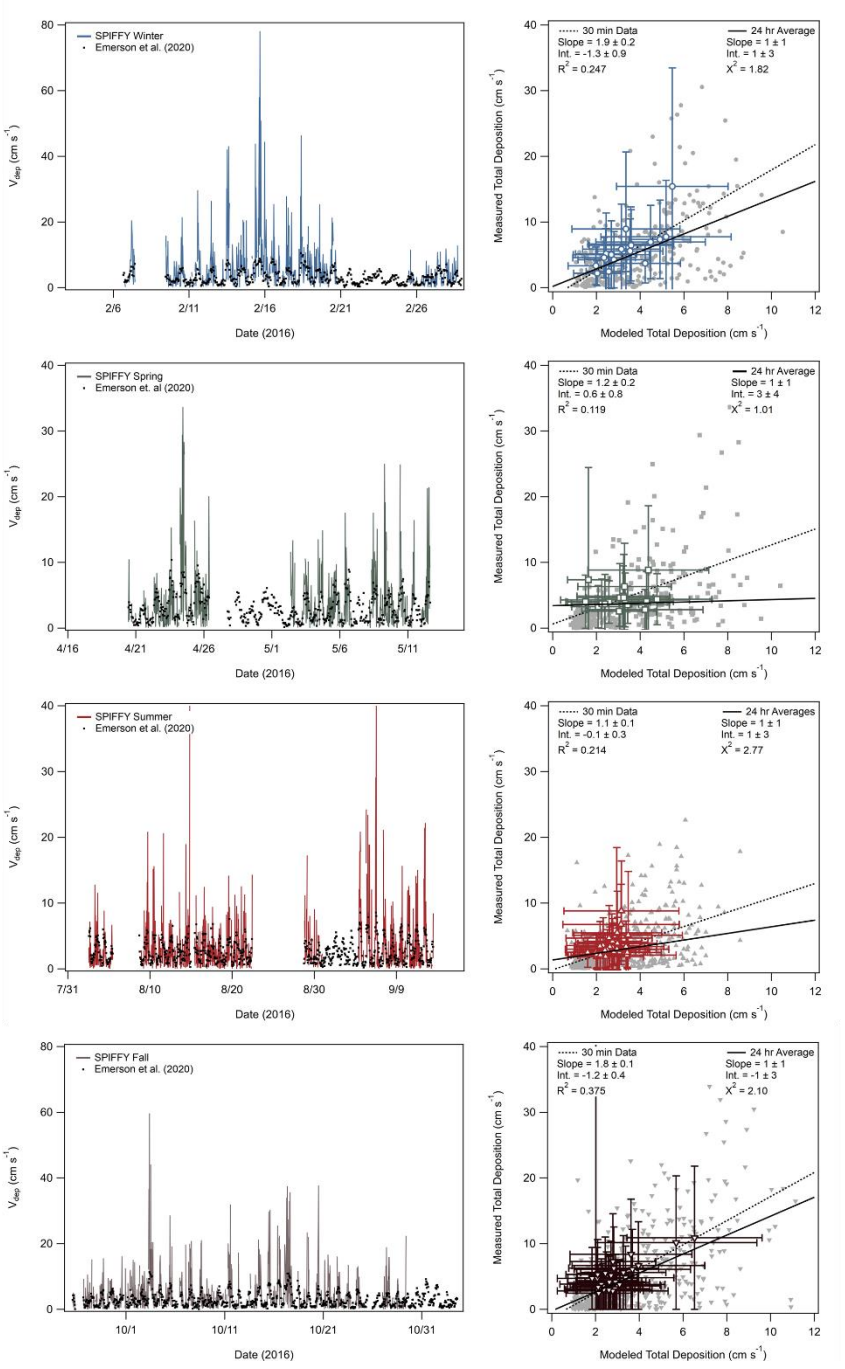


**Figure S12**: Comparison of total measured deposition velocity versus the output of the Emerson et al. (2020) model for total deposition. Timeseries comparisons are shown on the left while linear fits of the measured versus modeled deposition velocity are presented on the right for the 30-minute raw data and 24-hour averages. The 24-hour averages obscure the comparison between the measured and modeled values.

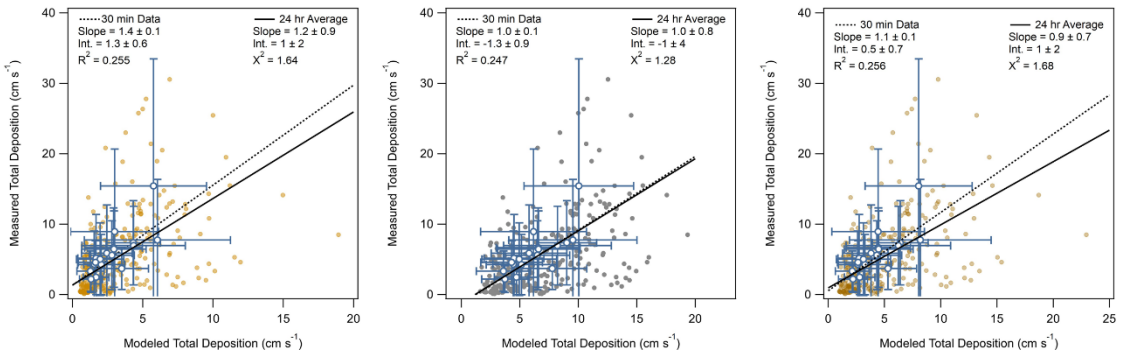


**Figure S13**: Comparison of total measured deposition velocity versus (left) the output of the Emerson et al. (2020) model with the turbophoresis term from form Katul et al. (2010) incorporated and (middle) the output of the Emerson et al. (2020) model with an altered interception term increasing its influence during the wintertime. The comparison of total measured deposition velocity versus (right) the output of the Emerson et al. (2020) model with the turbophoresis term from form Katul et al. (2010) and the interception term scaled up is also shown.

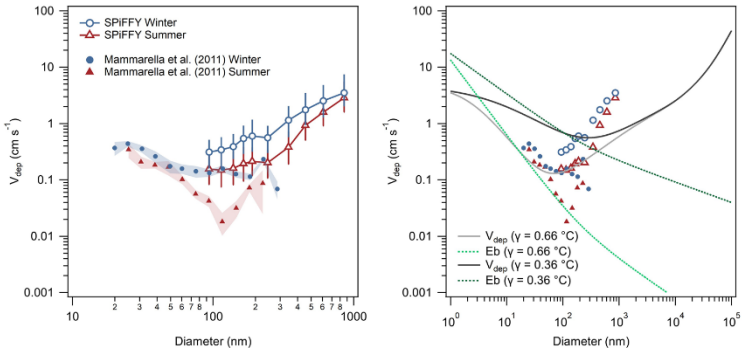


**Figure S14**: Comparison of SPiFFY winter and summer data to the seasonal data from Mammarella et al. (2011) (left), and the incorporation of the suppressed γ value measured by Mammarella et al. (2011) into the Emerson et al. (2020) model (right). This change significantly changes the predicted size-dependent deposition velocity. The shift in the minimum created by the change is not supported by other deposition velocity measurements and does nothing to improve model and measurement agreements in the SPiFFY data.

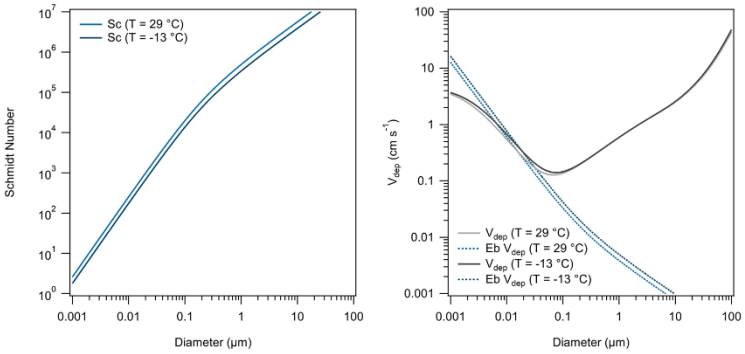


**Figure S15**: Temperature dependence of the Schmidt number (left) and its effect on the Brownian collection efficiency and deposition velocity (right). These temperatures span the range of the highest and lowest reported temperatures during the SPiFFY campaign.

**References**

Emerson, E. W., Hodshire, A. L., DeBolt, H. M., Bilsback, K. R., Pierce, J. R., McMeeking, G. R., and Farmer, D. K.: Revisiting particle dry deposition and its role in radiative effect estimates, PNAS, https://doi.org/10.1073/pnas.2014761117, 2020.

Katul, G. G., Grönholm, T., Launiainen, S., and Vesala, T.: Predicting the dry deposition of aerosol-sized particles using layer-resolved canopy and pipe flow analogy models: Role of turbophoresis, 115, https://doi.org/10.1029/2009JD012853, 2010.

Mammarella, I., Rannik, Ü., Aalto, P., Keronen, P., Vesala, T., and Kulmala, M.: Long-term aerosol particle flux observations. Part II: Particle size statistics and deposition velocities, Atmospheric Environment, 45, 3794–3805, https://doi.org/10.1016/j.atmosenv.2011.04.022, 2011.